Temperature Impact on Lithium Metal Morphology in Lithium Reservoir-Free Solid-State Batteries

Min-Gi Jeong[†] and Kelsey B. Hatzell[*]
Andlinger Center for Energy and the Environment, Princeton University, 86 Olden Avenue, Princeton, New Jersey 08650, USA

Sourim Banerjee, Bairav S. Vishnugopi, and Partha P. Mukherjee
School of Mechanical Engineering, Purdue University, 585 Purdue Mall, West Lafayette, Indiana 47907, USA

(Received 4 February 2024; revised 2 April 2024; accepted 18 April 2024; published 17 May 2024)

Lithium reservoir-free solid-state batteries can offer exceedingly high energy densities for a range of emerging applications related to aviation and electric vehicles. However, reversible operation of reservoir-free cells is plagued by a range of degradation mechanisms. The morphology of lithium metal film and subsequent evolution during operation can be highly variable and is dependent on the type of solid electrolyte, current collector, and operating conditions (current density, temperature, pressure, etc.). Here we evaluate lithium metal vertical and horizontal growth mechanisms at an argyrodite solid electrolyte–stainless steel interface at various temperatures from 25 to 80 °C. Combining confocal imaging and mesoscale modeling, we demonstrate how lithium metal island agglomeration is accelerated at elevated temperatures and facilitates greater horizontal growth of lithium metal. Maintaining high active material contact (e.g., horizontal growth) is critical for the formation of reversible lithium metal anodes in reservoir-free cells.

DOI: 10.1103/PRXEnergy.3.023003

I. INTRODUCTION

Removing excess non-charge-storing materials in a battery is one route to increase the cell-level energy density. Removal of inactive components such as binders, current collectors, and additives can reduce the overall weight and volume of the cell, leading to increases in the gravimetric and volumetric energy density. Another route to increase the cell-level energy density is to reduce the electrode loading such that 100% of the active material cycles during every charge and discharge cycle. This is sometimes referred to as an anode-free, low N/P ratio, or a lithium reservoir-free cell [1–5].

Solid-state lithium reservoir-free cells contain a solid electrolyte, a lithiated (discharged) cathode, and two current collectors [6,7]. During operation, ions deintercalate from the cathode and plate onto the anodic current collector during charge and form a lithium metal anode electrode. This process alleviates the need for expensive lithium manufacturing [8] and may enable a fabrication route for processing thin lithium metal foils (25 μm or less) [9–11].

Despite the promise of lithium reservoir-free solid-state batteries, there are numerous challenges that prevent high rate operation and long cycle lifetime. Notably, lithium nucleation processes can result in nonuniform films and the formation of isolated islands of Li [2,8,12]. Theoretical investigations have suggested that the isolated lithium island structures can generate mechanical stresses that impact the overpotential and growth mechanisms [13]. Furthermore, the work of adhesion between lithium metal and the solid electrolyte has been theoretically and experimentally linked to nucleation size, suggesting that tailored interactions between cell components may provide a pathway for controlling the properties and structure of the electroplated lithium metal electrode [8]. Electrodeposition in a lithium reservoir-free solid-state battery results in two major long-range effects: (1) stress generation at interfaces and (2) dynamic changes in active contact surface area. Constrained lithium deposits can grow horizontally to alleviate stress generation and maintain a high contact area or can grow vertically and induce large stress gradients and decrease the active contact area [14,15].

[*]Corresponding author: kelsey.hatzell@princeton.edu
[†]Also at Department of Mechanical and Aerospace Engineering, Princeton University, 86 Olden Street, Princeton, NJ 08544, USA.

Kayzak *et al.* [2] recently demonstrated through a combined theoretical and experimental investigation that the horizontal growth mechanism is enhanced at elevated pressures and active area contact is optimized via the use of thicker and more rigid current collectors. Fuchs *et al.* [4] corroborated this finding and demonstrated how the plating morphology is impacted by operating current density. Higher current densities resulted in an increase in particle density and active area coverage. In addition, to current density, operating temperature has also been shown to impact the active contact area and size of nuclei during deposition. Motoyama *et al.* [16] demonstrated how the nucleation overpotential and density of nuclei decreased with increasing temperature at LiPON|Cu interfaces.

Operating conditions related to pressure, current density, and temperature can all change the contact area between the solid electrolyte and the plated metal and the morphological evolution of the lithium metal. Increasing the operating temperature will alter the mechanical properties of the lithium metal and the subsequent stress distribution at the current collector. This study investigates vertical and horizontal lithium metal growth mechanisms against an argyrodite Li_6PS_5Cl (LPSC) solid electrolyte in a reservoir-free lithium solid-state battery at different operating temperatures. Prior studies examined nucleation dynamics on LiPON and LLZO ($Li_{6.24}La_3Zr_2Al_{0.24}O_{11.98}$), but little is known about the dynamics of long-range lithium metal growth on argyrodite LPSC solid electrolyte. Combining confocal imaging with mesoscale modeling, we track horizontal and vertical growth mechanisms. Deposition of lithium at a stainless steel (SS)-LPSC interface at different temperatures reveals film growth processes distinctly different from what was previously observed at elevated temperatures for LiPON thin film solid-state batteries. Lithium island size decreases with increasing temperature and horizontal growth dominates. While initial nucleus size and distribution play a role in electrode growth, chemomechanical interactions between the solid electrolyte, the metal, and the current collector have a greater role in determining electrode morphology at higher capacities [17,18]. Elevated temperatures lead to an increase in morphological stability. At elevated temperatures, lithium islands demonstrate greater agglomeration and a smoother reaction front.

II. EXPERIMENTAL METHODS

Lithium reservoir-free solid-state cells (Li|LPSC|SS) were assembled to visualize horizontal and vertical growth. Lithium foil was initially positioned on the bottom of the cell holder and then solid electrolyte (LPSC) at a density of 125 mg cm^{-2} was loaded and compressed at a force of 370 MPa. After compression of the solid electrolyte, a stainless steel current collector was introduced and subjected to a pressure of 50 MPa. This entire assembly process was performed within an argon-saturated dry glove box. Electrodeposition experiments using a BioLogic potentiostat were conducted at 0.1 mA cm^{-2} (1 mA h cm^{-2}) under a stack pressure of 1 MPa at 25, 60, and 80 °C.

The surface morphology of the deposited Li on the stainless steel current collector was observed with scanning electron microscopy (Verios 460 XHR, FEI Corporation). A confocal microscope (VK-X3050, Keyence) was used to analyze the change in the thickness and particle size of the deposited Li. Electrodes were physically separated from the electrolyte and then immersed in *N*-methyl-2-pyrrolidone solvent to completely dissolve the LPSC on the surface and dried for analysis.

III. RESULTS AND DISCUSSION

A. Temperature impact on electrodeposition of reservoir-free solid-state batteries

The growth of lithium metal upon electrodeposition has a significant impact on the reversible operation of a reservoir-free solid-state battery. Drastic morphological and microstructural dynamics during electrodeposition and dissolution contribute to the low rate capability of these devices [19]. Operating conditions such as temperature and pressure can influence the density, morphology, and texturing of the lithium metal electrode. Currently, reversible operation of reservoir-free solid-state batteries is hampered by short cycle lifetime and small capacities. Half-cells composed of a lithium metal working electrode and a stainless steel counter electrode separated by an argyrodite (LPSC) solid electrolyte (Li|LPSC|SS) were assembled to investigate the impact of temperature on electrodeposition dynamics. The voltage profile during electrodeposition (lithium plating) at a current density of 0.1 mA cm^{-2} demonstrates a characteristic peak followed by a voltage plateau [Fig. 1(a)]. The voltage peak is indicative of lithium nucleation, and the difference between the plateau voltage and the peak voltage is referred to as the "nucleation overpotential." The nucleation overpotential decreases with temperature [Fig. 1(b)]. At 25 °C, the nucleation overpotential is 0.046 V, with a higher initial peak and a lower plateau voltage. As the temperature increases to 60 and 80 °C, the nucleation overpotential decreases to 0.031 and 0.025 V, respectively. Increasing the temperature makes the substrate (or current collector) more lithiophilic and enables faster diffusion of the lithium ions to the surface [20–22]. Both these dynamics can impact the size of the nuclei and growth pattern during electrodeposition.

Lithium tends to form nonuniform nucleus sizes on stainless steel at 25 °C [Fig. 1(c)]. Nucleated lithium forms aggregates that are several microns or larger in diameter. As the temperature increases, the aggregation size becomes more uniform and flat. The high-temperature lithiophilic

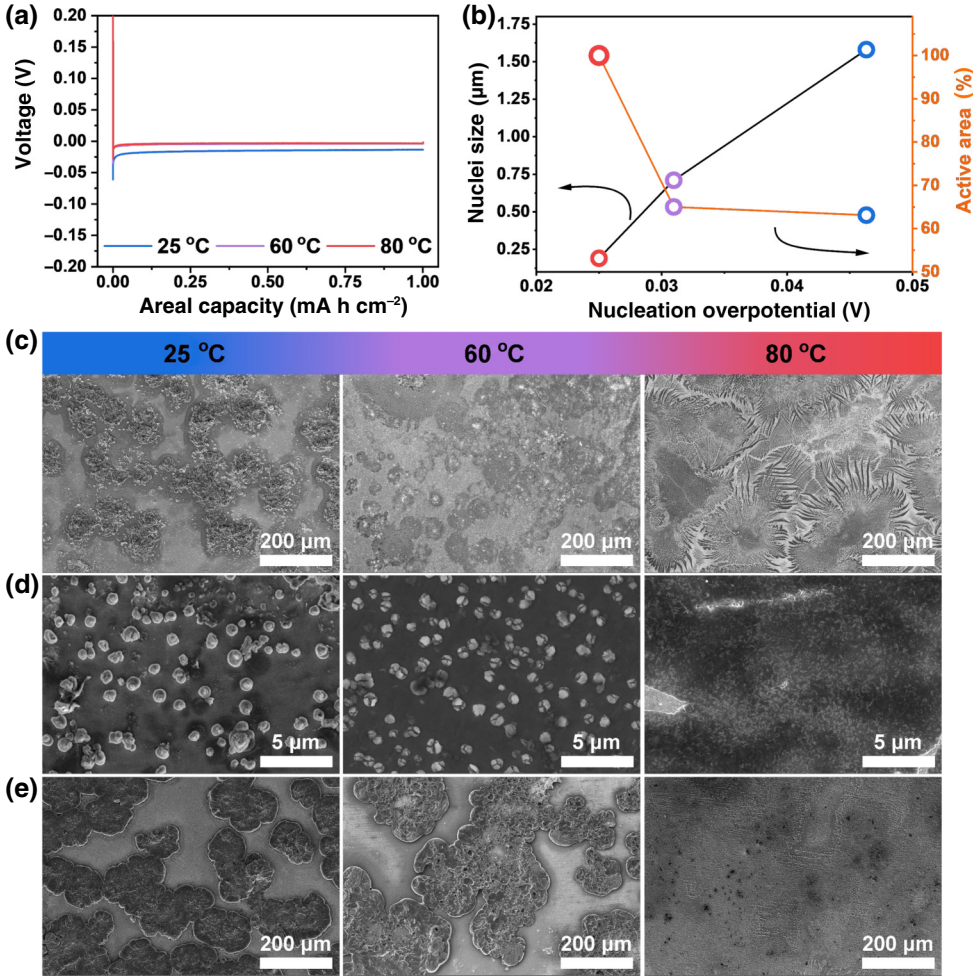

FIG. 1. Examination of the influence of temperature on lithium deposition, (a) Voltage profiles corresponding to differing temperatures. (b) Trends in the size of Li nuclei and the associated active area as influenced by temperature. Scanning electron microscopy images of the morphology of Li deposited at a capacity of 0.1 mA h cm^{-2} (c) at low magnification and (d) at high magnification. (e) Li deposited at a capacity of 1 mA h cm^{-2}.

substrate leads to lithium spreading dynamics and the formation of a filmlike morphology [Fig. 1(c)]. Individual nucleation points are observed with high-magnification scanning electron microscopy at 25 and 40 °C [Fig. 1(d)]. No nuclei were apparent in the high-temperature plating. The nucleus size and size distribution decrease with increasing temperature. At 25 °C, there is a large size distribution with an average nucleus size of around 1.58 μm [Fig. S1 in Supplemental Material [23] and Fig. 1(b)]. At 60 °C, the nucleus size becomes more uniform, at around 0.71 μm. Finally, at 80 °C, the average nucleus size is around 0.19 μm (Fig. S1 in Supplemental Material [23]).

Increasing the temperature leads to smaller nuclei at solid-solid interfaces and more uniform coverage across the current collector. This can play a significant role in the film growth mechanism. Scanning electron microscopy was conducted after deposition of lithium at 1 mA h cm^{-2} to explore this growth process further [Fig. 1(e)]. At low temperatures (25 °C) and medium temperatures (60 °C), we observe the formation of a nonuniform film comprising "islandlike" structures. These islands are interconnected and range from 100 to 500 μm in length. Conversely, at 80 °C, a uniform film was formed [Fig. 1(e)]. Higher-resolution imaging reveals that the film is not completely smooth but is visibly rough [Fig. S2(c) in Supplemental Material [23]].

Lithium deposition in a reservoir-free solid-state battery occurs between the solid electrolyte and the current collector. Lithium nucleus initiation and growth processes can lead to nonuniform growth that will result in nonuniform contact between the electrochemical active surface area and the solid electrolyte. Nonuniform contact can contribute to a smaller active surface area, local increases in the current flux, and constriction effects [24–26]. Ideally, lithium would grow horizontally (at a constant thickness) to form a uniform film. However, our observations suggest

that the vertical growth (e.g., electrode thickness) and horizontal growth (e.g., electrode diameter) mechanisms may differ depending on the current density and temperature. To understand the growth process (e.g., vertical versus horizontal), we monitored how the active contact area changes with capacity plated. We designate the "active area" as regions of contact between the electrode (e.g., plated lithium metal) and the solid electrolyte. Segmentation of the scanning electron microscopy images allowed direct quantification of the active area [Figs. 1(b) and 1(e) and Fig. S2 in Supplemental Material [23]]. The active area is a indicator of the preferred horizontal growth process and tends to increase with temperature. The active area was 63% at 25 °C, 67% at 60 °C, and 100% at 80 °C. Smaller and more uniform nucleation tends to lead to more uniform lithium films.

Confocal microscopy imaging was used to further capture and explore the vertical and horizontal growth mechanisms during electrodeposition in a reservoir-free solid-state battery. Black particles were observed on the stainless steel after plating at 0.1 mA h cm^{-2} at 25 °C [Fig. 2(a)]. These particles increased in size as the capacity increased from 0.1 to 1 mA h cm^{-2}. The plated particles coalesce into a spherical shape with a diameter of around 100 μm at 1 mA h cm^{-2} and 25 °C. This result aligns with the scanning electron microscopy observations [Fig. 1(e)], which demonstrates the lithium cannot form a uniform film under these conditions. In contrast, a flat and smooth film is observed with large area coverage for plating at 0.1 mA h cm^{-2} at 60 °C. Plating at an elevated temperature (80 °C) leads to the growth of a uniform lithium metal film after plating of lithium at 1 mA h cm^{-2}. There is a linear relationship between the plated capacity and plated particle size [Fig. 2(d)]. At 25 °C, plated particles on the order of 41.6 μm are initially observed and increase in site to 131 μm at an areal capacity of 1 mA h cm^{-2}. At 60 °C, there was an initial formation of a horizontal film with a size of 170 μm. This initial flat growth may be related to the field of view of the imaging. Nevertheless, vertical deposits become apparent when lithium was plated at 0.25 mA h cm^{-2}. The plated lithium radius is smaller at 60 °C than at 25 °C. As the capacity plated increases, large spherical clusters start to emerge. The growth progression differs between 25 and 60 °C. At 25 °C, small clustering is observed, leading to a film with a greater number of discontinuities [Fig. 2(a)]. At 60 °C, lithium starts to form large spherical clusters [Fig. 2(b)]. At 80 °C, the film appears to be uniformly

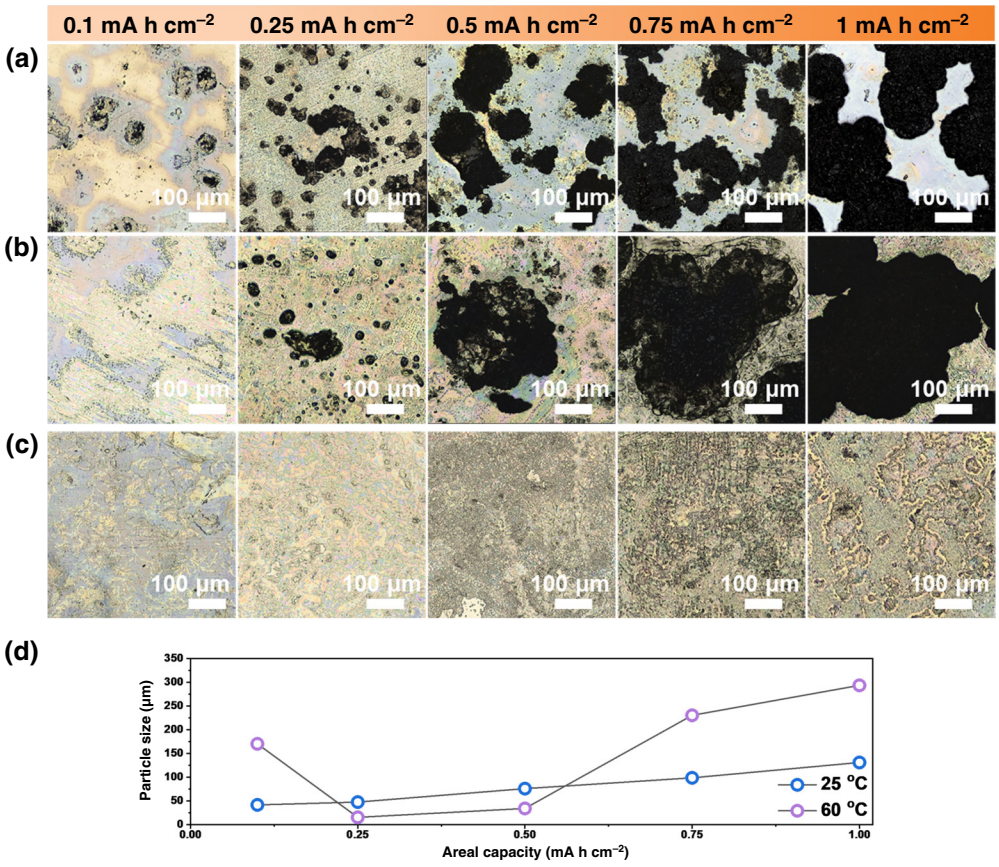

FIG. 2. Optical microscopy images of lithium deposited at low to high areal capacity at (a) 25 °C, (b) 60 °C, and (c) 80 °C. (d) Quantified growth trajectory of lithium islands on the electrode during the first deposition process.

connected and thin throughout the entire plating process [Fig. 2(c)].

B. Confocal imaging of lithium metal vertical and lateral growth

Three-dimensional confocal microscopy aids our understanding of the vertical and lateral growth mechanisms (Fig. 3). Blue regions represent valleys (small film thickness) and red regions represent peaks (large film thickness). Line profiles of the confocal images reveal the large variability in film thickness throughout the field of view (Fig. S4 in Supplemental Material [23]). Use of a confocal microscope allows the acquisition of images at different heights through z stacking. However, this means there are limitations in accurately determining the thickness of samples that do not have variations in height. Li deposition at 80 °C results in a uniform layer of lithium with no observable changes in thickness [Fig. 3(a)]. This makes it impossible to measure the thickness. However, after deposition at 1 mA h cm^{-2}, the thickness of the lithium was observed to be 5 μm, suggesting that the growth was consistent with theoretical values (theoretical value 5 μm at 1 mA h cm^{-2}) (Fig. S5 in Supplemental Material [23]).

The vertical growth increases with increasing plating capacity and decreasing temperature [Fig. 3(b)]. Plating of lithium at 0.1 mA h cm^{-2} at 25 °C results in an average film thickness of around 1.71 μm (Fig. S4 in Supplemental Material [23]). If the plating is uniform and continuous, the theoretical film thickness should be approximately 0.5 μm. The large difference suggests a highly heterogeneous film with low connectivity of active material. The film thickness doubles to 3.62 μm at 25 °C after plating of lithium metal at 0.25 mA h cm^{-2}. Between 0.25 and 1 mA h cm^{-2} there is a large increase in the thickness (17.37 μm at 0.5 mA h^{-2}). This sudden jump in thickness suggests that after a period of plating, the dominant growth mechanisms is in the vertical direction.

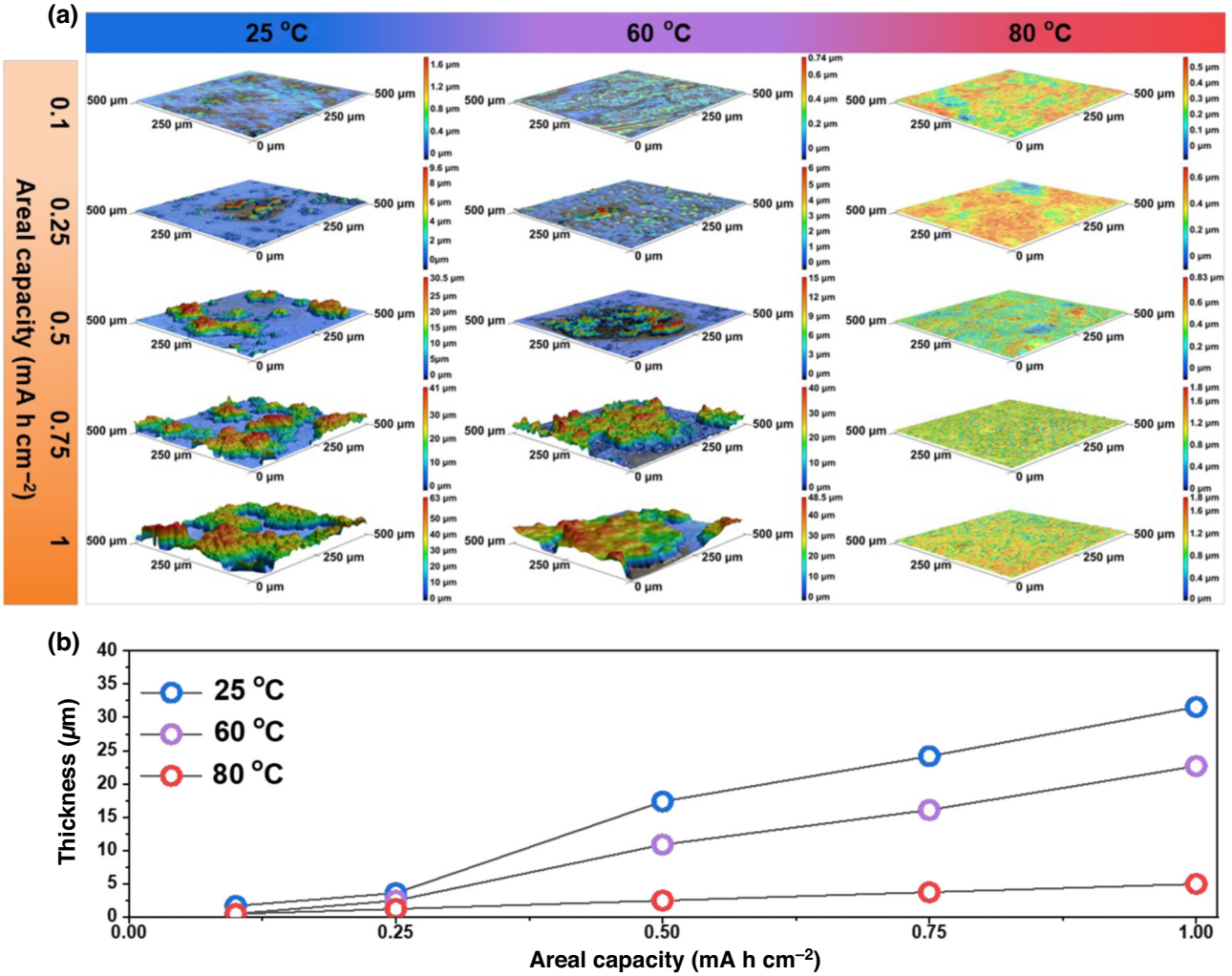

FIG. 3. (a) Three-dimensional morphology map of the electrode, revealing changes with temperature as the plating capacity increases from 0.1 to 1 mA h cm^{-2}. (b) Quantitative analysis of the correlation between Li deposition thickness and areal capacity.

At 60 °C, the thickness was around the theoretical thickness (0.54 μm) after plating at 0.1 mA h cm^{-2}. However, the film thickness diverges from the theoretical thickness at around 0.5 mA h cm^{-2}. The theoretical thickness of a uniform film plated at 0.5 mA h cm^{-2} should be around 2.5 μm. The measured thickness was nearly 4 times the theoretical thickness for a uniform film (10.9 μm) at 60 °C. Thus, at 25 and 60 °C, there is significant vertical growth after plating of lithium metal at 0.5 mA h cm^{-2}.

The results suggest that lithium grows horizontally initially but primarily grows in the vertical direction at high capacities. The operating pressure (e.g., compression) is not high enough to limit this vertical growth. Instead, *ex situ* analysis suggests that lithium metal can grow into the solid electrolyte and deform the interface. Increasing the temperature reduces the vertical growth. The film thickness decreases from 14.2 μm (25°) to around the theoretical minimum thickness of 5 μm at 80 °C (Fig. S5 in Supplemental Material [23]) after plating of lithium metal at 1 mA h cm^{-2}. This indicates a decrease in the vertical growth rate as temperatures increase. This finding implies there is greater lateral expansion at the higher temperature, a conclusion that aligns with the results shown in Fig. 2.

C. Mesoscale modeling of lithium morphology changes with temperature

To understand the underlying effect of temperature on the morphological growth during electrodeposition, we develop a mesoscale model based on the kinetic Monte Carlo method that captures the competing interaction between ionic transport, surface self-diffusion of Li, and electrochemical reaction at the electrode-electrolyte interface [27]. To probe the temperature dependence of the Li morphology, an electrochemical Biot number (Bi $\propto k_R/k_T$), Eq. (S6) in Supplemental Material [23], is defined on the basis of the ratio of the reaction rate k_R and the ionic transport rate k_T. In this analysis, the transport rate is kept constant; hence, any change in Bi directly correlates with a variation in the reaction rate.

A detailed description of the modeling framework and parameters is presented in Supplemental Material [23]. Simulations were conducted until a 2000 Li atoms had been deposited. Figure 4(a) shows the morphological tip height during electrodeposition as a function of Bi and temperature. While there is an increase in the tip height at higher values of Bi, the electrodeposition morphology is significantly stabilized at higher temperatures. As observed in Figs. 4(b)–4(e), the Li morphology transitions from mossy to filmlike as the temperature is increased from 25 to 80 °C. The increase in the morphological stability with temperature [Fig. 4(a)] is driven by the enhanced propensity for agglomeration of early-stage electrodeposits and the dynamic evolution of smoother reaction fronts. Specifically, the increase in the surface self-diffusion (k_D) of Li plays a critical role in this stabilizing mechanism, as governed by the following Arrhenius expression:

$$k_D = \nu \exp\left(\frac{-E_a}{k_B T}\right), \tag{1}$$

where ν is the hopping frequency, E_a is the activation barrier for the surface migration of Li, k_B is the Boltzmann constant, and T is the temperature. The thermal enhancement of self-diffusion facilitates the homogenization of the reaction rate at the interface, and mitigates the onset of hot spots that can lead to filament growth. In addition, the synergistic improvement in ionic transport with increasing temperature results in a uniform flux distribution in the vicinity of the interface, thereby promoting the dynamic growth of a filmlike deposition morphology. Building on the current mesoscale model, which captures the coupled effect of ion transport, Li diffusion, and interfacial reaction on the electrodeposition morphology, we will incorporate the influence of mechanical stresses at the interface into this framework in future work.

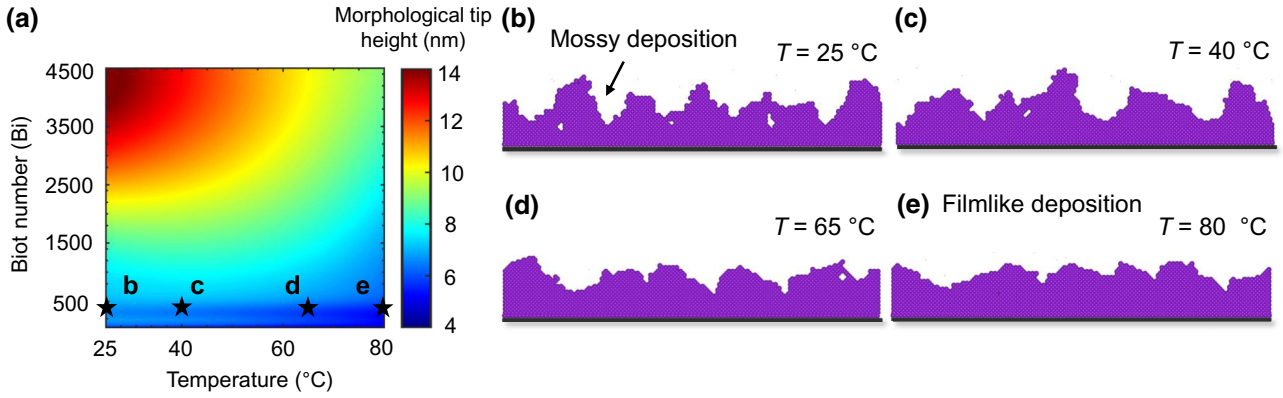

FIG. 4. (a) Morphological tip height as a function of the electrochemical Biot number Bi and temperature. Electrodeposition morphologies captured by the mesoscale model at (b) 25 °C, (c) 40 °C, (d) 65 °C, and (e) 80 °C.

D. Conclusions

Reservoir-free cells require reversible cycling of 100% of the active material within a battery. The growth of a lithium metal anode upon deposition and subsequent depletion of that film during stripping can lead to complex morphological changes. Most notably, the absence of a liquid electrolyte can lead to a decrease in the active contact area between the current collector and the solid electrolyte if lithium metal prefers to grow vertically instead of horizontally. The growth of lithium metal in the horizontal direction is strongly tied to the mechanical properties of the lithium metal and the current collector. Combining confocal imaging and mesoscale modeling, we show that lithium islands are more likely to agglomerate into a horizontal film at elevated temperatures. Improved surface diffusion of lithium metal and a smoother reaction front enable the fabrication of electrodes with uniform thicknesses and morphologies.

ACKNOWLEDGMENTS

This material is based on research supported by the Office of Naval Research under Award No. N00014-22-1-2406S. K.B.H. acknowledges support from the National Science Foundation (Grants No. 2041505 and No. 2140472). P.P.M. acknowledges financial support from the Office of Naval Research (ONR) (Grant No. N00014-23-1-2608). P.P.M. and K.B.H. would like to thank Dr. Michele Anderson from ONR for supporting this work.

[1] C. Haslam and J. Sakamoto, Stable lithium plating in "lithium metal-free" solid-state batteries enabled by seeded lithium nucleation, J. Electrochem. Soc. **170**, 040524 (2023).

[2] E. Kazyak, M. J. Wang, K. Lee, S. Yadavalli, A. J. Sanchez, M. Thouless, J. Sakamoto, and N. P. Dasgupta, Understanding the electro-chemo-mechanics of Li plating in anode-free solid-state batteries with *operando* 3D microscopy, Matter **5**, 3912 (2022).

[3] K. B. Hatzell, Anode-less or anode-free?, ACS Energy Lett. **8**, 4775 (2023).

[4] T. Fuchs, J. Becker, C. G. Haslam, C. Lerch, J. Sakamoto, F. H. Richter, and J. Janek, Current-dependent lithium metal growth modes in "anode-free" solid-state batteries at the Cu—LLZO interface, Adv. Energy Mater. **13**, 2203174 (2023).

[5] J. A. Lewis, S. E. Sandoval, Y. Liu, D. L. Nelson, S. G. Yoon, R. Wang, Y. Zhao, M. Tian, P. Shevchenko, E. Martínez-Pañeda, *et al.*, Accelerated short circuiting in anode-free solid-state batteries driven by local lithium depletion, Adv. Energy Mater. **13**, 2204186 (2023).

[6] T. Krauskopf, F. H. Richter, W. G. Zeier, and J. Janek, Physicochemical concepts of the lithium metal anode in solid-state batteries, Chem. Rev. **120**, 7745 (2020).

[7] K. B. Hatzell, X. C. Chen, C. L. Cobb, N. P. Dasgupta, M. B. Dixit, L. E. Marbella, M. T. McDowell, P. P. Mukherjee, A. Verma, V. Viswanathan, *et al.*, Challenges in lithium metal anodes for solid-state batteries, ACS Energy Lett. **5**, 922 (2020).

[8] M. J. Wang, E. Carmona, A. Gupta, P. Albertus, and J. Sakamoto, Enabling "lithium-free" manufacturing of pure lithium metal solid-state batteries through in situ plating, Nat. Commun. **11**, 5201 (2020).

[9] M. J. Wang, E. Kazyak, N. P. Dasgupta, and J. Sakamoto, Transitioning solid-state batteries from lab to market: Linking electro-chemo-mechanics with practical considerations, Joule **5**, 1371 (2021).

[10] K. B. Hatzell and Y. Zheng, Prospects on large-scale manufacturing of solid state batteries, MRS Energy Sustain. **8**, 33 (2021).

[11] M. B. Dixit, W. Zaman, Y. Bootwala, Y. Zheng, M. C. Hatzell, and K. B. Hatzell, Scalable manufacturing of hybrid solid electrolytes with interface control, ACS Appl. Mater. Interfaces **11**, 45087 (2019).

[12] B. Neudecker, N. Dudney, and J. Bates, "lithium-free" thin-film battery with in situ plated Li anode, J. Electrochem. Soc. **147**, 517 (2000).

[13] M. Motoyama, M. Ejiri, and Y. Iriyama, Modeling the nucleation and growth of Li at metal current collector/LiPON interfaces, J. Electrochem. Soc. **162**, A7067 (2015).

[14] A. J. Sanchez, E. Kazyak, Y. Chen, J. Lasso, and N. P. Dasgupta, Lithium stripping: anisotropic evolution and faceting of pits revealed by *operando* 3-D microscopy, J. Mater. Chem. A **9**, 21013 (2021).

[15] A. L. Davis, E. Kazyak, D. W. Liao, K. N. Wood, and N. P. Dasgupta, Operando analysis of interphase dynamics in anode-free solid-state batteries with sulfide electrolytes, J. Electrochem. Soc. **168**, 070557 (2021).

[16] M. Motoyama, M. Hirota, T. Yamamoto, and Y. Iriyama, Temperature effects on Li nucleation at Cu/LiPON interfaces, ACS Appl. Mater. Interfaces **12**, 38045 (2020).

[17] P. Albertus, S. Babinec, S. Litzelman, and A. Newman, Status and challenges in enabling the lithium metal electrode for high-energy and low-cost rechargeable batteries, Nat. Energy **3**, 16 (2018).

[18] M. B. Dixit, B. S. Vishugopi, W. Zaman, P. Kenesei, J.-S. Park, J. Almer, P. P. Mukherjee, and K. B. Hatzell, Polymorphism of garnet solid electrolytes and its implications for grain-level chemo-mechanics, Nat. Mater. **21**, 1298 (2022).

[19] D. K. Singh, T. Fuchs, C. Krempaszky, B. Mogwitz, and J. Janek, Non-linear kinetics of the lithium metal anode on Li_6PS_5Cl at high current density: Dendrite growth and the role of lithium microstructure on creep, Adv. Sci. **10**, 2302521 (2023).

[20] K. Yan, J. Wang, S. Zhao, D. Zhou, B. Sun, Y. Cui, and G. Wang, Temperature-dependent nucleation and growth of dendrite-free lithium metal anodes, Angew. Chem. **131**, 11486 (2019).

[21] W. Zaman, L. Zhao, T. Martin, X. Zhang, Z. Wang, Q. J. Wang, S. Harris, and K. B. Hatzell, Temperature and pressure effects on unrecoverable voids in Li metal solid-state batteries, ACS Appl. Mater. Interfaces **15**, 37401 (2023).

[22] L. Zhao, Q. J. Wang, X. Zhang, K. B. Hatzell, W. Zaman, T. V. Martin, and Z. Wang, Laplace-fourier transform solution to the electrochemical kinetics of a symmetric lithium cell affected by interface conformity, J. Power Sources **531**, 231305 (2022).

[23] See the Supplemental Material at http://link.aps.org/supplemental/10.1103/PRXEnergy.3.023003 additional data and statistics and information on modeling.

[24] J. K. Eckhardt, P. J. Klar, J. Janek, and C. Heiliger, Interplay of dynamic constriction and interface morphology between reversible metal anode and solid electrolyte in solid state batteries, ACS Appl. Mater. Interfaces **14**, 35545 (2022).

[25] J. K. Eckhardt, T. Fuchs, S. Burkhardt, P. J. Klar, J. Janek, and C. Heiliger, Guidelines for impedance analysis of parent metal anodes in solid-state batteries and the role of current constriction at interface voids, heterogeneities, and SEI, Adv. Mater. Interfaces **10**, 2202354 (2023).

[26] A. Pei, G. Zheng, F. Shi, Y. Li, and Y. Cui, Nanoscale nucleation and growth of electrodeposited lithium metal, Nano Lett. **17**, 1132 (2017).

[27] B. S. Vishnugopi, F. Hao, A. Verma, and P. P. Mukherjee, Surface diffusion manifestation in electrodeposition of metal anodes, Phys. Chem. Chem. Phys. **22**, 11286 (2020).